



Synthesis of a MIMO QFT controller for hydraulic hybrid swing system of excavators*

Yan Cai^a, Jinchun Song^a and Nariman Sepehri^b

^aSchool of Mechanical Engineering and Automation, Northeastern University, Shenyang, China; ^bDepartment of Mechanical Engineering, University of Manitoba, Winnipeg, Canada

ABSTRACT

In swing system of excavators, energy recuperation and hybrid actuation is desirable to improve energy efficiency because of its characteristic large inertial load and cyclic operation. Numerous studies have focused on optimisation of hybrid structures and power management strategies, whereas only a little attention has been paid to the control performance of hybrid swing drives. This paper investigates the control problem of the secondary controlled hybrid swing drive and employs multi-input multi-output quantitative feedback theory (MIMO QFT) for controller synthesis. Considering parametric uncertainties in load variation, viscous friction and bulk modulus, a two-input two-output QFT control scheme is constructed according to specifications given by robust margin, sensitivity reduction and tracking performance. Through simulation evaluation, the MIMO QFT controller shows excellent tracking performance over the defined range of uncertain parameters and much better robustness as compared to a well-tuned PI controller. The synthesis process is visualised, which is practical and promising for its further use in industrial settings.

ARTICLE HISTORY

Received 11 September 2016
Accepted 7 August 2017

KEYWORDS

MIMO QFT; secondary control; hydraulic hybrid swing; uncertainty; excavator

1. Introduction

Excavators are extensively used in various kinds of earth-work construction sites. Faced with challenges posed by fuel consumption and exhaust emissions, efficiency improvement of excavator powertrain systems is in high demand (Vukovic and Murrenhoff 2015).

Given the large inertial load and cyclic operation, it is ideal to implement energy recuperation and hybrid actuation on excavators (Pettersson 2009). Energy recuperation is achieved by storing rotational kinetic energy or potential energy with energy storage devices and then reusing it for acceleration. Hybrid actuation implies more than one power sources are utilised in a system. Normally, a diesel engine is chosen as the prime mover, and energy storage devices, such as batteries, capacitors and accumulators, are used as backup power sources. A hybrid powertrain system using regenerative energy can compensate for power deficiency at peak operating points, which will ultimately cut down the engine size and improve fuel efficiency. According to Lin *et al.* (2010a) in a typical digging duty cycle, potential energy in the boom and kinetic energy in the swing circuits constitute most of the recoverable fuel consumption.

Among numerous original design manufacturers, Kobelco developed a 6-ton hybrid excavator to cut energy consumption by 40% (Kagoshima *et al.* 2007).

Komatsu proposed a hybrid excavator with electric storage devices, which reduced up to 41% of fuel consumption (Inoue 2008). However, these hybrid excavators use electric motors with large rated power and corresponding storage devices. They are costly with low power density (Pettersson and Tikkanen 2009). The large and frequent variation in load power also makes the batteries or capacitors work in severe conditions, which makes the expected life cycle a serious issue (Ochiai and Ryu 2008). Caterpillar (2012) commercialised an excavator with hydraulic hybrid swing system, to capture the swing braking energy of the upper structure in accumulators, and then release the energy during swing acceleration.

In academia, Wang *et al.* (2005) conducted a simulation study evaluating energy efficiency of series and parallel electric hybrid schemes applied to excavators. Xiao *et al.* (2008) investigated several control strategies of power system on electric hybrid excavators and proposed a dynamic-work-point control scheme. Tae-Suk Kwon *et al.* (2010) compared three structures for a hybrid excavator with a supercapacitor, and proposed a power control algorithm for the engine and the supercapacitor. Yoon *et al.* (2013) proposed an electric hybrid scheme on a 5-ton excavator with each hydraulic actuator driven by an electric motor/generator. Researchers at Purdue University (Williamson *et al.* 2008, Zimmerman *et al.*

CONTACT Nariman Sepehri  nariman.sepehri@umanitoba.ca

*This work was completed in the Fluid Power and Tele-Robotics Research Laboratory at University of Manitoba.

2011, Hippalgaonkar and Ivantysynova 2013) implemented a series–parallel hydraulic hybrid displacement controlled scheme on a 5-ton prototype excavator with optimal power management to improve fuel economy.

While most studies have focused on hybrid structures and power management strategies of the powertrain to optimise fuel consumption, only a few studies have examined dynamic control issues of hybrid excavators (Jin *et al.* 2012). Hybrid power systems were first successfully implemented on automobiles, which are quite different from those on construction machinery. Due to large and frequent load fluctuation and also the configuration of multi-actuators, dynamic control of hybrid excavators is more challenging than that of hybrid vehicles (Lin *et al.* 2010b).

With excellent dynamics and capacity of energy recuperation, a secondary controlled hydraulic hybrid swing drive is a notable technology for energy efficient excavators. As shown in Figure 1, it is composed of a primary unit (variable displacement pump) and a secondary unit (variable displacement pump/motor) with corresponding charging circuits. Through displacement control of the primary unit, the system working pressure can be regulated without throttling losses. Meanwhile, either position or velocity of the excavator rotating part can be controlled by regulating the displacement of the secondary unit. Additionally, energy recuperation and reutilisation can be achieved through control of accumulator's state of charge. The secondary unit can behave as either a motor or a pump depending on operation and loading situation.

Since the introduction of this concept, a number of studies were conducted on actuator position, velocity or torque control, but only to achieve low performances due to the open-loop structure or the high nonlinearity. To improve static and dynamic performances and to facilitate the implementation, Berg and Ivantysynova (1999) proposed a position and velocity control scheme for a secondary controlled hydraulic drive assuming constant working pressure. Pettersson and Tikkanen (2009) outlined the potential of secondary control in an excavator swing drive and discussed safety concepts to handle system failures. Ho and Ahn (2012) implemented

a hierarchal control strategy on an energy regenerative closed-loop hydrostatic transmission and designed an adaptive fuzzy sliding mode controller for speed control of the secondary unit. To overcome the limitation of assuming constant high operating pressure, Busquets and Ivantysynova (2014) synthesised a robust multi-input multi-output (MIMO) H-infinity controller for the control of swing velocity and the accumulator's state of charge. To improve the position and velocity tracking performance, Busquets and Ivantysynova (2015) further proposed an adaptive robust controller for motion control of the secondary controlled hydraulic hybrid swing system.

A secondary controlled hydraulic hybrid swing drive is characterised as fast dynamics, high power density and unrestricted four-quadrant operation. It is capable of recuperating energy and has better energy efficiency as compared to a valve-controlled hydraulic system. In spite of all the advantages, secondary controlled hydraulic hybrid drives are found in few industrial applications, which is mainly due to the complexity of control schemes (Pettersson 2009).

In most construction sites, unknown operating and loading modes cause time-variant swing inertia in a duty cycle, which subsequently induce variations in working pressure, friction properties and bulk modulus (Yao *et al.* 1998). Different environmental stiffness and rapidly changing ground slope also cause swing torque variation, which are time-variant, not easy to describe and ultimately captured on system pressure and load velocity. They should be considered as external disturbances to be suppressed. Although excavators are normally designed with an intentional load sensitivity to give operator feedback as to the applied force, this undoubtedly sacrifices the excavators' control performance, especially when the load varies drastically. Whereas in teleoperated or automated excavation, force feedback signals are adopted to give the operator or supervisor clear information about the interaction with the unknown environment. Therein, minimising load sensitivity is required to maintain robust control performance against various environment. All these issues form uncertainties and make it ideal for implementing the practical frequency domain method, quantitative feedback theory (QFT), for controller design to achieve robust performances of the hydraulic hybrid swing drive. With parametric uncertainties and desired specifications shown on Nichols chart quantitatively, the design process and also trade-offs between performances and controller complexity can be visualised, which is very useful in practice. Note that a secondary controlled hydraulic hybrid swing system is a two-input two-output configuration in nature. Therefore, it is necessary to investigate the implementation of MIMO QFT. According to Lee *et al.* (2000), other available MIMO robust synthesis approaches, such as μ -synthesis, do not always have all the desired properties. Such controllers

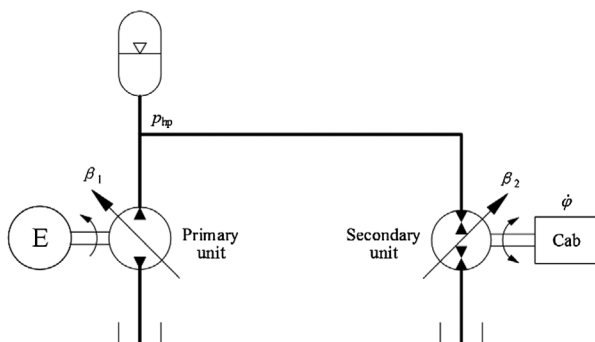


Figure 1. Schematic diagram of secondary controlled hydraulic hybrid swing system (Busquets and Ivantysynova 2014).

may have exceedingly high orders and exhibit resonances or instability. The use of weights with increasing orders for tuning purposes may not be as transparent as QFT tuning which does not involve weights and is executed directly on the open-loop frequency response. Advantages of using QFT over H-infinity design procedure have also been addressed by Chait and Hollot (1990).

This paper is aimed to propose a MIMO QFT controller synthesis approach for hydraulic hybrid swing system of excavators. Considering parametric uncertainties in load variation, viscous friction and bulk modulus, a two-input two-output QFT diagonal control scheme can be constructed to meet specifications given by robust margin, sensitivity reduction and tracking. During the process, environmental interferences are considered as output disturbances to be suppressed. Through simulation evaluation, the corresponding controller performances are verified based on both step and time-variant reference inputs. Compared with previous studies, through quantifying and visualisation in the design process, the two-input two-output QFT diagonal control scheme greatly reduces the design complexity. Meanwhile, excellent tracking performance and robustness are achieved.

The rest of this paper is organised as follows. Modelling of the hydraulic hybrid swing drive is presented in Section 2. QFT design framework is introduced in Section 3. A two-input two-output QFT diagonal control scheme for the secondary controlled hydraulic hybrid swing system is synthesised in Section 4. Simulation evaluation of the proposed controller is carried out in MATLAB/SIMULINK environment in Section 5. Conclusions are given in Section 6.

2. Modelling hydraulic hybrid swing system

Modelling of the system is based on the state space description by Busquets and Ivantysynova (2014).

The pressure buildup equation of the secondary controlled hydraulic hybrid swing drive can be expressed as:

$$\dot{p}_{\text{hp}} = \frac{1}{C_{\text{H}}} \left(n_1 V_1 \beta_1 \eta_1 - \frac{n_2 V_2 \beta_2}{\eta_2} \right) \quad (1)$$

where p_{hp} is the working pressure of the high pressure chamber, n_1 and n_2 are the speeds of the primary and secondary units, V_1 and V_2 are the corresponding maximum volumetric displacements, β_1 and β_2 are the normalised proportion of the maximum displacements, η_1 and η_2 are the unit volumetric efficiencies considering internal and external leakages, and C_{H} is the hydraulic capacitance, due to fluid compressibility and the accumulator.

The rotating part of the excavator, including the cab, linkages, payload, etc., is herein referred to as the upper structure. The dynamics of the upper structure can be described as:

$$\ddot{\varphi} = \frac{1}{J} \left(\frac{V_2 p_{\text{hp}} i_{\text{TOT}} \eta \beta_2}{2\pi} - b\dot{\varphi} - T_{\text{nf}} \right) \quad (2)$$

where J is the combined inertia of the upper structure, which varies with the posture and payload, φ is the angular position of the upper structure, i_{TOT} is the total gear ratio between the secondary unit and the upper structure, η is the mechanical efficiency of the secondary unit, b is the viscous friction coefficient, and T_{nf} is the non-linear friction considering Stribeck effect. With reference to Armstrong and Canudas de Wit (1995), T_{nf} can be expressed as:

$$T_{\text{nf}} = (T_{\text{c}} + (T_{\text{brk}} - T_{\text{c}})e^{(-c_v|\dot{\varphi}|)})\text{sign}(\dot{\varphi}) \quad (3)$$

where T_{c} is the Coulomb friction torque, T_{brk} is the breakaway friction torque, c_v is a transition approximation coefficient.

Since the combined dynamics of the control valve and the swash plate is generally much faster than that of the hybrid swing system, they can be ignored. Besides, the non-linear friction, T_{nf} is neglected for the purpose of linearisation. Its effects are to be constrained to some extent in disturbance rejection at the controller design stage, which will be verified in Section 5. To avoid numerical errors in computation, a scaling factor, S_c is introduced such that $\bar{p}_{\text{hp}} = p_{\text{hp}}/S_c$. It is noted that $n_2 = \dot{\varphi} i_{\text{TOT}}/(2\pi)$. Given input $\mathbf{u} = [u_1, u_2]^T = [\beta_1, \beta_2]^T$, output $\mathbf{y} = [y_1, y_2]^T = [\bar{p}_{\text{hp}}, \dot{\varphi}]^T$, and state variables defined as $\mathbf{x} = [x_1, x_2]^T = [\bar{p}_{\text{hp}}, \dot{\varphi}]^T$, the state space model of the secondary controlled hydraulic hybrid swing drive is then described as:

$$\dot{x}_1 = \frac{1}{C_{\text{H}} S_c} \left(n_1 V_1 \eta_1 u_1 - \frac{V_2 i_{\text{TOT}} x_2 u_2}{2\pi \eta_2} \right) \quad (4)$$

$$\dot{x}_2 = \frac{1}{J} \left(\frac{V_2 i_{\text{TOT}} \eta S_c x_1 u_2}{2\pi} - b x_2 \right) \quad (5)$$

Utilising Taylor series expansion and neglecting the higher order constant infinitesimals, the linearised state space model in matrix form is expressed as:

$$\begin{bmatrix} \dot{x}_1 \\ \dot{x}_2 \end{bmatrix} = \mathbf{A} \begin{bmatrix} x_1 \\ x_2 \end{bmatrix} + \mathbf{B} \begin{bmatrix} u_1 \\ u_2 \end{bmatrix} \quad (6)$$

$$\begin{bmatrix} y_1 \\ y_2 \end{bmatrix} = \mathbf{C} \begin{bmatrix} x_1 \\ x_2 \end{bmatrix} + \mathbf{D} \begin{bmatrix} u_1 \\ u_2 \end{bmatrix} \quad (7)$$

$$\text{where } \mathbf{A} = \begin{bmatrix} 0 & -\frac{V_2 i_{\text{TOT}} u_{2\text{ref}}}{2\pi C_{\text{H}} \eta_2 S_c} \\ \frac{V_2 i_{\text{TOT}} \eta S_c u_{2\text{ref}}}{2\pi J} & -\frac{b}{J} \end{bmatrix}, \mathbf{B} = \begin{bmatrix} \frac{n_1 V_1 \eta_1}{C_{\text{H}} S_c} & -\frac{V_2 i_{\text{TOT}} x_{2\text{ref}}}{2\pi C_{\text{H}} \eta_2 S_c} \\ 0 & \frac{V_2 i_{\text{TOT}} \eta S_c x_{1\text{ref}}}{2\pi J} \end{bmatrix},$$

$$\mathbf{C} = \begin{bmatrix} 1 & 0 \\ 0 & 1 \end{bmatrix}, \text{ and } \mathbf{D} = \begin{bmatrix} 0 & 0 \\ 0 & 0 \end{bmatrix}.$$

Table 1. Nominal values and uncertainty ranges of parameters.

Parameter	Symbol	Value	
		Range	Nominal
Maximum displacement of pump (m ³ /rev)	V_1	–	40×10^{-6}
Maximum displacement of motor (m ³ /rev)	V_2	–	40×10^{-6}
Total reduction ratio	i_{TOT}	–	60
Mechanical efficiency	η	–	0.8
Volumetric efficiency of the pump	η_1	–	0.9
Volumetric efficiency of the motor	η_2	–	0.9
Speed of the pump (rev/s)	n_1	–	40
Scaling factor	S_c	–	35×10^6
Rotating viscous coefficient (Nms/rad)	b	[5000, 15,000]	5000
Inertia of the upper structure (kgm ²)	J	[2000, 10,000]	2000
Hydraulic capacitance (m ³ /N)	C_H	$[1 \times 10^{-11}, 1 \times 10^{-10}]$	1×10^{-10}
Reference value of u_2	u_{2ref}	[-1, 1]	0
Reference value of x_1	x_{1ref}	[0.286, 1]	0.714
Reference value of x_2 (rad/s)	x_{2ref}	[-1, 1]	-0.0375

Therefore, the plant transfer function from \mathbf{u} to \mathbf{y} is represented as:

$$\mathbf{P} = \mathbf{C}(\mathbf{I}s - \mathbf{A})^{-1}\mathbf{B} + \mathbf{D} = \begin{bmatrix} s & \frac{V_2 i_{TOT} u_{2ref}}{2\pi C_H \eta_2 S_c} \\ -\frac{V_2 i_{TOT} n S_c u_{2ref}}{2\pi J} & s + \frac{b}{J} \end{bmatrix}^{-1} \begin{bmatrix} \frac{n_1 V_1 \eta_1}{C_H S_c} & -\frac{V_2 i_{TOT} x_{2ref}}{2\pi C_H \eta_2 S_c} \\ 0 & \frac{V_2 i_{TOT} n S_c x_{1ref}}{2\pi J} \end{bmatrix} \quad (8)$$

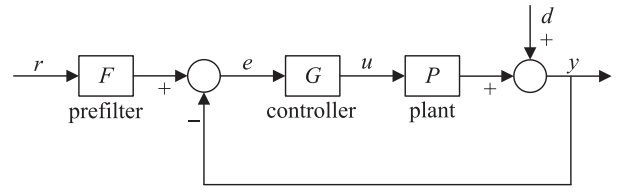
The nominal values of parameters and their uncertainty ranges used in controller synthesis and simulation analyses are listed in Table 1. Note that some of the system parameters are adopted from Busquets and Ivantysynova (2014), i.e. b , J , S_c , C_H , η , u_{2ref} , x_{1ref} , x_{2ref} . However, some other parameters involved in their controller design are not fully specified. Based on excavators' technical data and the authors' experience, the values of V_1 , V_2 , n_1 , i_{TOT} , η_1 and η_2 are specified as in Table 1.

3. QFT

QFT is a frequency domain method for designing a low bandwidth robust controller to achieve desired plant output responses in the presence of plant uncertainties and unknown disturbances (Yaniv 1999). As this design technique is graphically based, QFT can quantitatively show the exact levels of plant uncertainty, desired specifications and control efforts on Nichols chart. In turn, designers can obtain a direct insight into the trade-offs among them and prevent overdesign while formulating design iterations through the QFT Toolbox (Borghesani *et al.* 2003). In this section, SISO QFT controller design framework is described, followed by extension to MIMO QFT problem. Note that the notations used by Yaniv (1999) are adopted.

3.1. SISO QFT problem

A typical two DOF single-input single-output (SISO) unity feedback system is depicted in Figure 2, consisting of a plant P , a controller G and a pre-filter F . d is the disturbance at the plant output.

**Figure 2.** Single-input single-output two DOF unity feedback system with output disturbance.

When designing a controller, usually one or more typical performance specifications are selected to conduct the synthesis according to requirements.

- (1) Robust margin: the gain and phase margin is bounded by $\left| \frac{PG}{1+PG} \right| \leq m(\omega)$, for $\omega \geq \omega_m$;
- (2) Sensitivity reduction (output disturbance rejection): the transfer function from the disturbance at the plant output to the plant output is bounded by $\left| \frac{1}{1+PG} \right| \leq \alpha(\omega)$, for $\omega \leq \omega_s$;
- (3) Tracking performance: the transfer function from the reference signal to the plant output is bounded by $a(\omega) \leq \left| F \frac{PG}{1+PG} \right| \leq b(\omega)$, for $\omega \leq \omega_{tr}$.

Since QFT is a frequency domain design technique, both the plant and the specifications should be described in frequency domain. At each given frequency, the response set of the plant family is referred to as a template, which is often obtained directly from frequency response measurements. Based on a selected nominal plant, open-loop bounds are quantitatively calculated at each frequency and shown on Nichols chart according to the given closed-loop specifications. Then designers can shape the open-loop frequency response to meet the desired bounds transparently at each given frequency to arrive at a controller. The process is known as loop shaping. Normally, the open-loop frequency response should remain at or above the open bounds and outside of the closed bounds at corresponding frequencies. For the tracking problem, a controller is designed to restrict the variation amplitude within the given range, and a pre-filter is also needed to shape the response into the

desired envelope to meet tracking performance. Due to approximations involved in the computation algorithm, controller design is usually followed by a detailed closed-loop analysis.

3.2. MIMO QFT problem

Extension to multi-input multi-output (MIMO) QFT problem is achieved by breaking the design process down into a series of stages. Each stage of the sequential process is simplified as a SISO feedback problem. The solution for the original problem is obtained by combining the controllers in each single loop. In terms of stability, it should be noted that in general, the poles of a closed-loop system are common to all those of transfer functions from any input to any output. Thus, stability is guaranteed if the last design stage is successfully executed.

A two-input two-output system, shown in Figure 3, is taken as an example to show the framework of MIMO QFT design. For all the upcoming problems,

$\mathbf{P} = \begin{bmatrix} p_{11} & p_{12} \\ p_{21} & p_{22} \end{bmatrix}$ is a 2×2 plant belonging to a set $\{\mathbf{P}\}$,

$\boldsymbol{\pi} = \begin{bmatrix} \pi_{11} & \pi_{12} \\ \pi_{21} & \pi_{22} \end{bmatrix}$ is the inverse of \mathbf{P} , $\mathbf{r} = [r_1, r_2]^T$ is the input vector, $\mathbf{y} = [y_1, y_2]^T$ is the output vector,

$\mathbf{d} = [d_1, d_2]^T$ is the disturbance vector, $\mathbf{G} = \begin{bmatrix} g_1 \\ g_2 \end{bmatrix}$

and $\mathbf{F} = \begin{bmatrix} f_{11} & f_{12} \\ f_{21} & f_{22} \end{bmatrix}$ are the controller and pre-filter to

be designed. Similar performance specifications as in SISO systems are defined to conduct the synthesis.

- (1) Robust margin: the gain and phase margin is bounded by $|1 + L_k(j\omega)|^{-1} \leq m_k(\omega)$, where L_k is the equivalent open-loop transfer function of the k th loop, $k = 1, 2$, $\omega \geq \omega_m$. Considering the coupling effects, the open-loop transfer function of each single loop is expressed as

$$L_1 = \frac{g_1}{\pi_{11}^2} = \frac{g_1}{\pi_{11} - \frac{\pi_{12}\pi_{21}}{\pi_{22} + g_2}} = \frac{g_1(\pi_{22} + g_2)}{|\boldsymbol{\pi}| + \pi_{11}g_2} \quad (9)$$

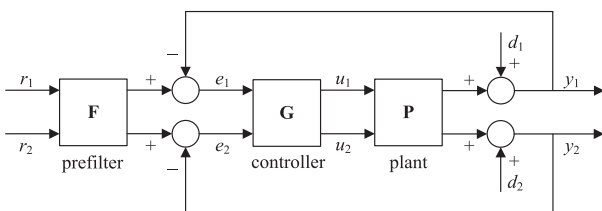


Figure 3. Two-input two-output two DOF unity feedback system.

$$L_2 = \frac{g_2}{\pi_{22}^2} = \frac{g_2}{\pi_{22} - \frac{\pi_{12}\pi_{21}}{\pi_{11} + g_1}} = \frac{g_2(\pi_{11} + g_1)}{|\boldsymbol{\pi}| + \pi_{22}g_1} \quad (10)$$

where π_{11}^2 (π_{22}^2) represents the equivalent inversed plant of the first (second) loop considering the coupling effect from the second (first) loop, which is obtained through LU decomposition.

To meet the robust margin constraint, for the first loop, the following inequality should be satisfied:

$$|1 + L_1|^{-1} = \left| \frac{|\boldsymbol{\pi}| + g_1\pi_{22} + g_2(\pi_{11} + g_1)}{|\boldsymbol{\pi}| + g_2\pi_{11}} \right|^{-1} \leq m_1(\omega) \quad (11)$$

Note that when $|g_2|$ approaches to 0, $\lim|1 + L_1|^{-1} = |1 + g_1p_{11}|^{-1} \leq m_1(\omega)$; when $|g_2|$ approaches to ∞ , $\lim|1 + L_1|^{-1} = |1 + g_1/\pi_{11}|^{-1} \leq m_1(\omega)$. These two inequalities can be directly used to calculate the robust margin bounds.

For the second loop, since the limit values of g_2 are used in the first loop design, g_2 should be designed to satisfy bounds calculated according to both the inequalities (11) and (12), i.e.

$$|1 + L_2|^{-1} = \left| 1 + \frac{g_2}{\pi_{22} - \frac{\pi_{12}\pi_{21}}{\pi_{11} + g_1}} \right|^{-1} \leq m_2(\omega) \quad (12)$$

- (2) Sensitivity reduction: the transfer function from the disturbance at the plant output to the plant output is bounded by $|s_{ij}(j\omega)| \leq \alpha_{ij}(\omega)$, $i, j = 1, 2$, $\omega \leq \omega_s$. The transfer function from \mathbf{d} to \mathbf{y} can be represented as $\mathbf{S} = (\mathbf{I} + \mathbf{P}\mathbf{G})^{-1}\mathbf{P}\mathbf{G}$. The equation is expressed in matrix as $\begin{bmatrix} \pi_{11} + g_1 & \pi_{12} \\ \pi_{21} & \pi_{22} + g_2 \end{bmatrix} \begin{bmatrix} s_{11} & s_{12} \\ s_{21} & s_{22} \end{bmatrix} = \begin{bmatrix} \pi_{11} & \pi_{12} \\ \pi_{21} & \pi_{22} \end{bmatrix}$.

Multiplying both sides by $\begin{bmatrix} 1 & 0 \\ \frac{-\pi_{21}}{\pi_{11} + g_1} & 1 \end{bmatrix}$ on the

left, it is obtained that

$$\begin{bmatrix} \pi_{11} + g_1 & \pi_{12} \\ 0 & \pi_{22}^2 + g_2 \end{bmatrix} \begin{bmatrix} s_{11} & s_{12} \\ s_{21} & s_{22} \end{bmatrix} = \begin{bmatrix} \pi_{11} & \pi_{12} \\ \pi_{21}^2 & \pi_{22}^2 \end{bmatrix} \quad (13)$$

where $\pi_{21}^2 = \pi_{21} - \frac{\pi_{21}\pi_{11}}{\pi_{11} + g_1}$ and $\pi_{22}^2 = \pi_{22} - \frac{\pi_{12}\pi_{21}}{\pi_{11} + g_1}$.

From Equation (13), the transfer function from each input to each output can be represented as:

$$s_{11} = \frac{\pi_{11} - \pi_{12}s_{21}}{\pi_{11} + g_1} \quad (14)$$

$$s_{12} = \frac{\pi_{12} - \pi_{12}s_{22}}{\pi_{11} + g_1} \quad (15)$$

$$s_{21} = \frac{\pi_{21}^2}{\pi_{22}^2 + g_2} \quad (16)$$

$$s_{22} = \frac{\pi_{22}^2}{\pi_{22}^2 + g_2} \quad (17)$$

To meet the sensitivity reduction specification, for the first loop, g_1 should satisfy the bounds given by

$$|s_{11}| \leq \left| \frac{|\pi_{11}| + |\pi_{12}|\alpha_{21}}{\pi_{11} + g_1} \right| \leq \alpha_{11}(\omega) \quad (18)$$

$$|s_{12}| \leq \left| \frac{|\pi_{12}| + |\pi_{12}|\alpha_{22}}{\pi_{11} + g_1} \right| \leq \alpha_{12}(\omega) \quad (19)$$

Note that Equations (14) and (15) do not follow the format of controller design in the QFT Toolbox, thus they are scaled into Equations (18) and (19) according to the subadditivity of absolute value.

For the second loop, g_2 can be designed according to the bounds described by the following inequalities:

$$|s_{21}| = \left| \frac{\pi_{21}^2}{\pi_{22}^2 + g_2} \right| \leq \alpha_{21}(\omega) \quad (20)$$

$$|s_{22}| = \left| \frac{\pi_{22}^2}{\pi_{22}^2 + g_2} \right| \leq \alpha_{22}(\omega) \quad (21)$$

- (3) Tracking performance: the transfer function from the reference signal to the plant output is bounded by $a_{ij}(\omega) \leq |t_{ij}(j\omega)| \leq b_{ij}(\omega)$, $i = 1, 2, j = 1, 2, \omega \leq \omega_r$. The transfer function from \mathbf{r} to \mathbf{y} is represented as $\mathbf{T} = (\mathbf{I} + \mathbf{P}\mathbf{G})^{-1}\mathbf{P}\mathbf{G}\mathbf{F} \rightarrow (\mathbf{I} + \mathbf{P}\mathbf{G})\mathbf{T} = \mathbf{P}\mathbf{G}\mathbf{F} \rightarrow (\mathbf{P}^{-1} + \mathbf{G})\mathbf{T} = \mathbf{G}\mathbf{F}$. It is expressed in matrix form as
- $$\begin{bmatrix} \pi_{11} + g_1 & \pi_{12} \\ \pi_{21} & \pi_{22} + g_2 \end{bmatrix} \begin{bmatrix} t_{11} & t_{12} \\ t_{21} & t_{22} \end{bmatrix} = \begin{bmatrix} g_1 & \\ & g_2 \end{bmatrix} \begin{bmatrix} f_{11} & f_{12} \\ f_{21} & f_{22} \end{bmatrix}.$$

Therefore, the transfer function from each input to each output can be represented as:

$$t_{11} = \frac{g_1 f_{11} - \pi_{12} t_{21}}{\pi_{11} + g_1} \quad (22)$$

$$t_{12} = \frac{g_1 f_{12} - \pi_{12} t_{22}}{\pi_{11} + g_1} \quad (23)$$

$$t_{21} = \frac{g_2 f_{21} - \pi_{21}^2 f_{11}}{\pi_{22}^2 + g_2} \quad (24)$$

$$t_{22} = \frac{g_2 f_{22} - \pi_{21}^2 f_{12}}{\pi_{22}^2 + g_2} \quad (25)$$

For the first loop, g_1 can be designed according to the bounds calculated by:

$$a_{11}(\omega) \leq \left| \frac{g_1 f_{11} \pm |\pi_{12}| b_{21}}{\pi_{11} + g_1} \right| \leq b_{11}(\omega) \quad (26)$$

$$a_{12}(\omega) \leq \left| \frac{g_1 f_{12} \pm |\pi_{12}| b_{22}}{\pi_{11} + g_1} \right| \leq b_{12}(\omega) \quad (27)$$

In this way, the problem is equivalent to two SISO two DOF problems with plant $1/\pi_{11}$, reference input $r_1 = \delta(t)$, and input disturbances as $|d_{11}| \leq |\pi_{12}| b_{21}$ and $|d_{12}| \leq |\pi_{12}| b_{22}$, respectively.

For the second loop, g_2 can be designed to satisfy the bounds given by:

$$a_{21}(\omega) \leq \left| \frac{g_2 f_{21} - \pi_{21}^2 f_{11}}{\pi_{22}^2 + g_2} \right| \leq b_{21}(\omega) \quad (28)$$

$$a_{22}(\omega) \leq \left| \frac{g_2 f_{22} - \pi_{21}^2 f_{12}}{\pi_{22}^2 + g_2} \right| \leq b_{22}(\omega) \quad (29)$$

This problem is equivalent to two SISO two DOF problems with plant $1/\pi_{22}^2$, reference input $r_2 = \delta(t)$, and input disturbances as $d_{21} = -\pi_{21}^2 f_{11}$ and $d_{22} = -\pi_{21}^2 f_{12}$, respectively.

4. Controller design

Following the MIMO QFT design procedure described earlier, a two-input two-output QFT diagonal control scheme is now synthesised for the hydraulic hybrid swing system. The performance specifications are defined as in Table 2. The tracking specifications are specified to meet the response performance with the maximum overshoot of 2% and settling time range of 0.1–0.9 s for p_{11} and p_{22} , considering a swing velocity of approximately 10 rev/min. The specifications of robust margin and sensitivity reduction are specified based on the authors' QFT design experience on other fluid power systems' applications. These performance specifications are believed to produce tight constraints to guide controller design considering the given uncertainty level.

The plant templates of p_{11} are obtained as in Figure 4 by calculating the frequency responses at each specific frequency based on the plant family with prescribed

Table 2. Performance specifications for controller design.

Performance	Constraints
Robust margin	$ 1 + L_p(j\omega) ^{-1} \leq 1.67, \omega \geq 0$ rad/s.
Sensitivity reduction	$ s_{ij}(j\omega) \leq 0.02\omega$, for $i = j$; $ s_{ij}(j\omega) \leq 0.01\omega$, for $i \neq j$. $\omega \leq 20$ rad/s.
Tracking	$a_{ij}(\omega) \leq t_{ij}(j\omega) \leq b_{ij}(\omega), \omega \leq 20$ rad/s. $a_{ij} = \frac{588.8}{(s+8)^2(s+9.2)}, b_{ij} = \frac{28.571(s+14)}{(s+20)^2}$ for $i = j$; $a_{ij} = 0, b_{ij} = 0.01\omega$ for $i \neq j$.

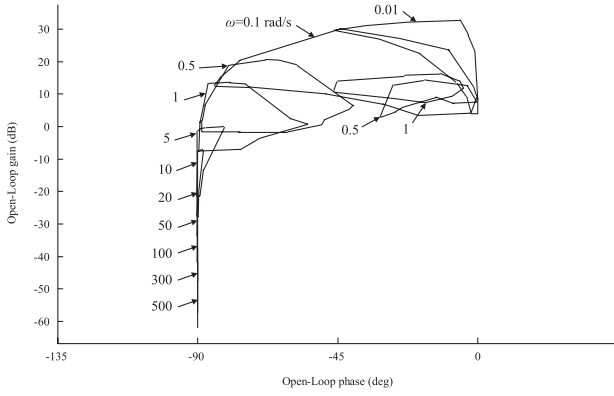


Figure 4. Plant templates of p_{11} .

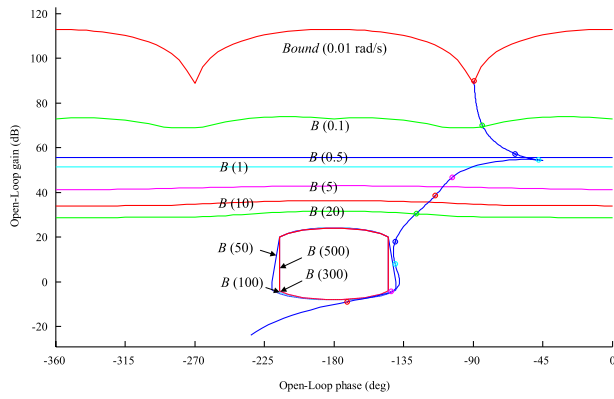


Figure 5. Selected bounds and nominal open-loop frequency response of p_{11} with the compensation of g_1 .

parametric uncertainties (see Table 1). It reveals the effect of uncertainties on system performance at each frequency and can be further used for controller design. The selected nominal plant for controller design is:

$$p_{110} = \frac{4.1143(s + 2.5)}{s^2 + 2.5s + 6.485} \quad (30)$$

Based on the nominal plant, open-loop bounds are calculated according to the three performance specifications and are selected to give the strictest constraints at each specific frequency. They are thereby referred to as selected bounds used for controller design. As is seen from Figure 5, the open bounds within 1 rad/s are calculated based on the tracking specifications; the open bounds between 1 and 20 rad/s are based on sensitivity reduction; and the closed bounds after 50 rad/s are corresponding to the robust margin constraint. An appropriate controller is required to shape the frequency response close to the bounds at low frequencies to prevent overdesign, and with a rapid attenuation after the transition frequency to reduce the impact of noise. Controller g_1 is then constructed by shaping the open-loop frequency response curve to fit the bounds at each specific frequency on the Nichols chart (i.e. introducing gains, poles and zeros to the controller) through trial and error:

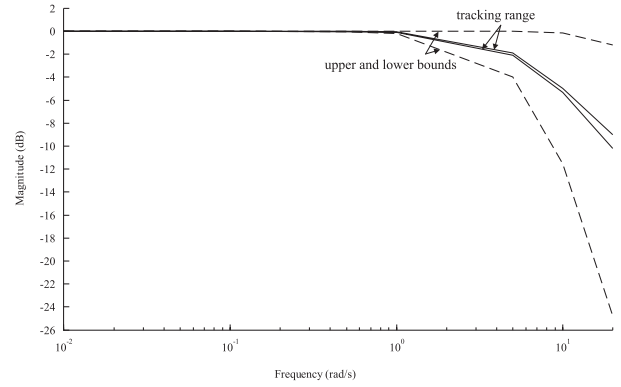


Figure 6. Pre-filter design for the first loop.

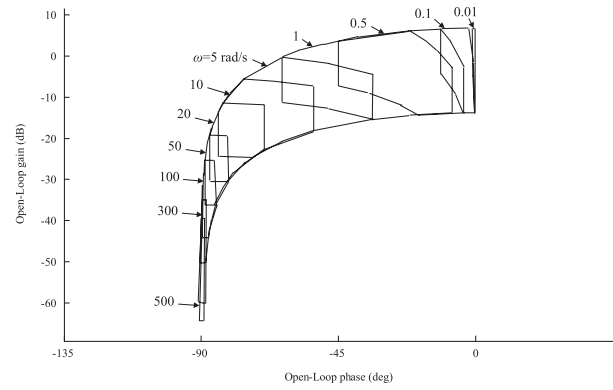


Figure 7. Plant templates of p_{22}^2 .

$$g_1 = \frac{1.3246 \times 10^7 (s + 0.9271)(s + 134.7)}{s(s + 23.19)(s^2 + 590.1s + 3.634 \times 10^5)} \quad (31)$$

Based on g_1 , a pre-filter f_{11} is designed to shape the closed-loop frequency responses into the desired envelope (see Figure 6), given by the tracking specifications. It is noted that to reduce calculation and meanwhile capture major variations of the frequency response curve, just a few proper frequencies rather than a dense frequency array are selected to conduct the pre-filter design.

$$f_{11} = \frac{6.376}{s + 6.376} \quad (32)$$

Note that when designing a controller for the first loop, the exact coupling effect from the second loop is unknown. Thus, approximations of the second loop are adopted and overdesign may have been introduced.

The templates of the equivalent plant for the second loop, p_{22}^2 , is shown in Figure 7. The selected nominal plant is:

$$p_{220}^2 = \left[\frac{1.5294(s^2 + 184.1s + 2.717 \times 10^4)}{(s + 2.511)(s^2 + 189.8s + 2.727 \times 10^4)} \right] \times \left[\frac{(s + 0.9324)(s^2 + 424.1s + 2.687 \times 10^5)}{(s + 0.9238)(s^2 + 422.6s + 2.69 \times 10^5)} \right] \quad (33)$$

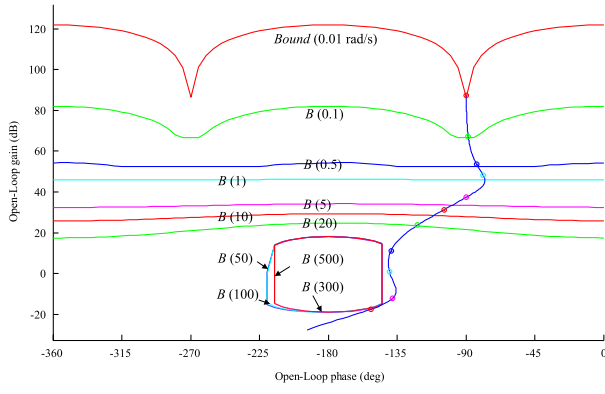


Figure 8. Selected bounds and nominal open-loop frequency response of p_{22}^2 with the compensation of g_2 .

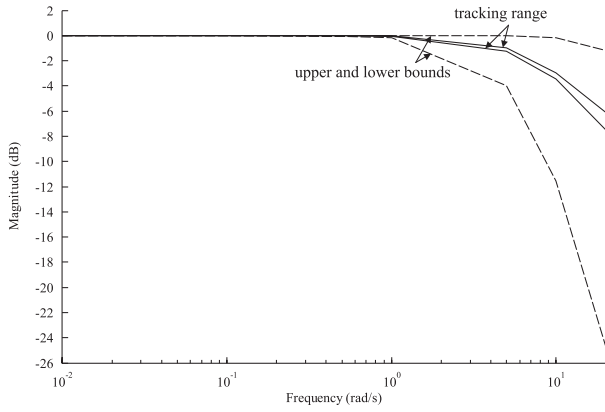


Figure 9. Pre-filter design of the second loop.

Based on the specified nominal plant, the open-loop bounds are calculated given the closed-loop specifications for the second loop (see Figure 8). Following the design principle, a controller g_2 is constructed:

$$g_2 = \frac{3.7015 \times 10^7 (s + 1.41)(s + 132.9)}{s(s + 22.81)(s^2 + 1372s + 8.087 \times 10^5)} \quad (34)$$

Given the compensation g_2 , the nominal open-loop frequency response of p_{22}^2 has been shaped to meet each bound at the given frequencies. The second loop control design has less approximation of coupling effects from the first loop. Thus, g_2 has less overdesign. Note that g_2 satisfies the stability of the second loop and thus guarantees the stability of the whole plant. Next, a pre-filter f_{22} is designed (see Figure 9) to meet the tracking performance of the second loop:

$$f_{22} = \frac{9.187}{s + 9.187} \quad (35)$$

The diagonal control scheme for the whole plant is obtained as:

$$\mathbf{G} = \begin{bmatrix} g_1 & \\ & g_2 \end{bmatrix} \quad (36)$$

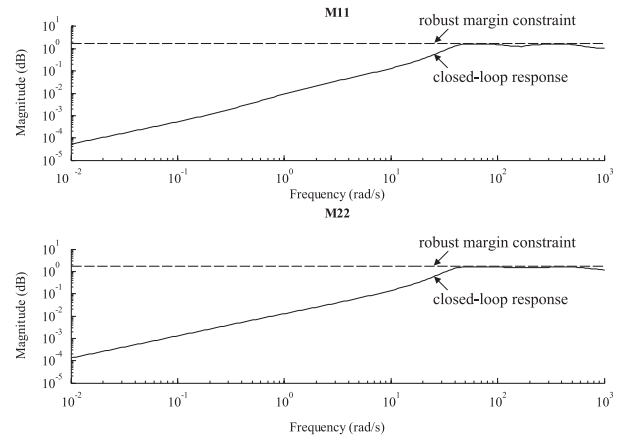


Figure 10. Robust margin analysis.

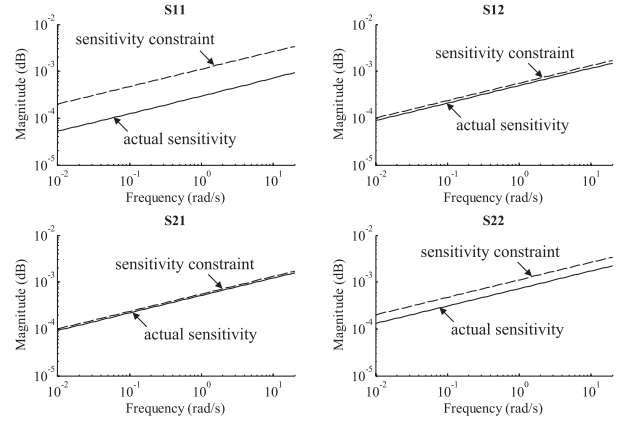


Figure 11. Sensitivity reduction analysis.

$$\mathbf{F} = \begin{bmatrix} f_{11} & \\ & f_{22} \end{bmatrix} \quad (37)$$

where controllers g_1, g_2 and pre-filters f_{11}, f_{22} are given by Equations (31), (34) and (32), (35), respectively.

Due to approximations involved in the calculation process, a closed-loop frequency response analysis with a denser frequency array is needed to check the performances once the controllers are designed. The worst scenario of the closed-loop responses with regard to uncertainties is chosen for demonstration according to the maximal magnitude.

In terms of robust margin, Figure 10 shows excellent results in both loops. Consistent with the loop shaping result, the tracking and sensitivity reduction constraints are dominant at low frequencies, and the robust margin bounds become dominant after 50 rad/s.

With respect to sensitivity reduction, results show good performance with the second loop (see Figure 11). Small overdesign is introduced to the first loop using the limit values of α_{21} and α_{22} in Equations (17) and (18). Note that since the robust margin performance has been satisfied, there is no need to alter the sensitivity in the first loop through iterations.

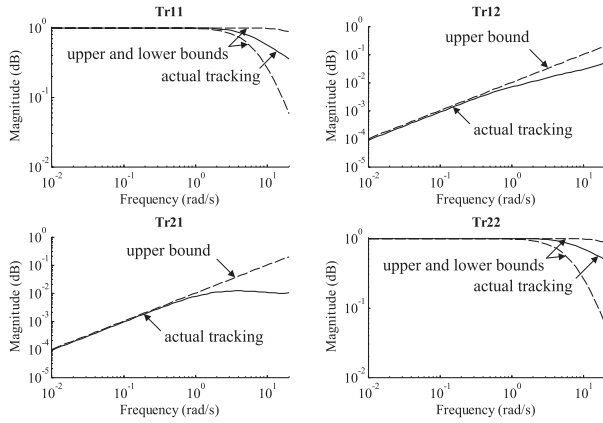


Figure 12. Tracking performance analysis.

Table 3. Randomly chosen parameters for robustness verification.

Groups	1	2	3	4	5
b (Nms/rad)	5000	5000	10000	15000	15000
J (kgm ²)	2000	10000	6000	2000	10000
C_H (m ⁵ /N)	1×10^{-10}	1×10^{-10}	5×10^{-11}	1×10^{-11}	1×10^{-11}
x_{1ref}	0.714	1	0.643	0.286	1
x_{2ref} (rad/s)	-0.0375	0.5	0	-0.5	-1
u_{2ref}	0	1	0	1	-1

As is seen from Figure 12, both T_{11} and T_{22} show good tracking performances within the desired envelope. Whereas T_{12} and T_{21} show good suppression of coupling interferences between every two channels.

The analysis of the control scheme is satisfying. We now need to further verify the performances through simulation using the entire system model.

5. Controller evaluations

In MATLAB/Simulink environment, given the diagonal control scheme described in Equations (36) and (37), the simulation evaluation and analysis are presented as follows.

5.1. Robustness verification against parameter uncertainty

A set of step reference signals with amplitudes of 1.2 MPa and 9 °/s, respectively, are adopted for pressure and velocity channels to verify the robust stability and tracking performance. System parameters of different levels are randomly grouped (see Table 3) to represent a wide range of loading situation.

As is seen from Figures 13 and 14, all the step responses are stable with no overshoot. The tracking specifications, 2% settling time of 0.1–0.9 s, are strictly satisfied for the plant family. In terms of the plant with nominal values, the 2% settling time for the pressure channel is 0.57 s and the steady-state error is 0.0037 MPa. The 2% settling time for the cabin velocity is 0.43 s, with a steady-state error of 0.0035 °/s. From Figure 15, it is seen that in

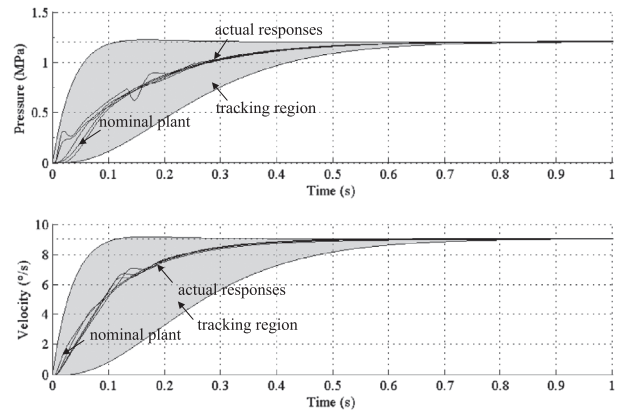


Figure 13. Tracking performances of the plant family with MIMO QFT control scheme given step reference inputs.

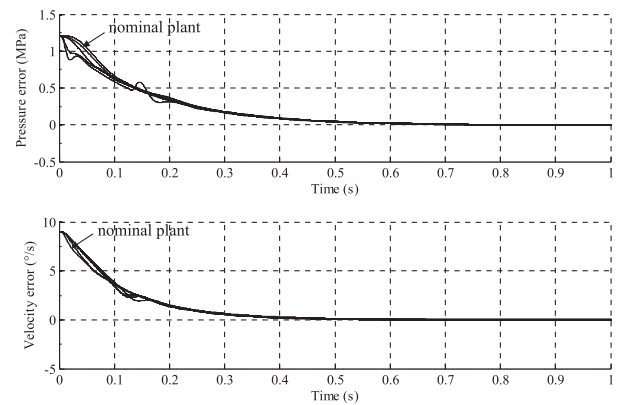


Figure 14. Tracking errors of the plant family with MIMO QFT control scheme given step reference inputs.

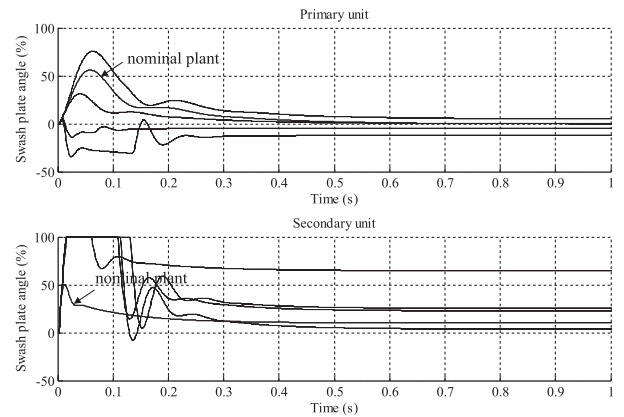


Figure 15. Swash plate angles of the plant family with MIMO QFT control scheme given step reference inputs.

each situation, the swash plate angles of both units are reasonable.

5.2. Robustness verification against output disturbances

To simulate the actual operating situation, actual field data presented by Busquets and Ivantysynova (2014) are reproduced as reference inputs to the hydraulic hybrid

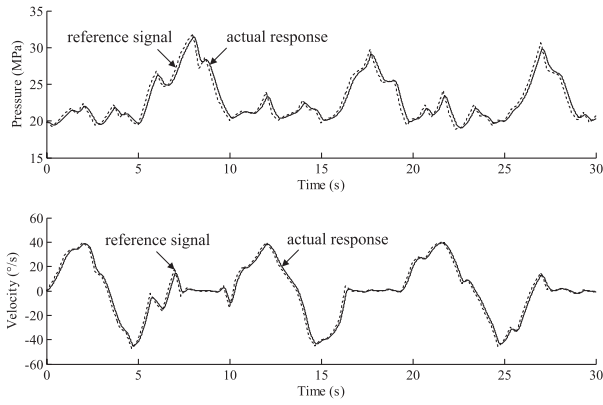


Figure 16. Tracking performances of MIMO QFT control scheme given time-variant reference inputs.

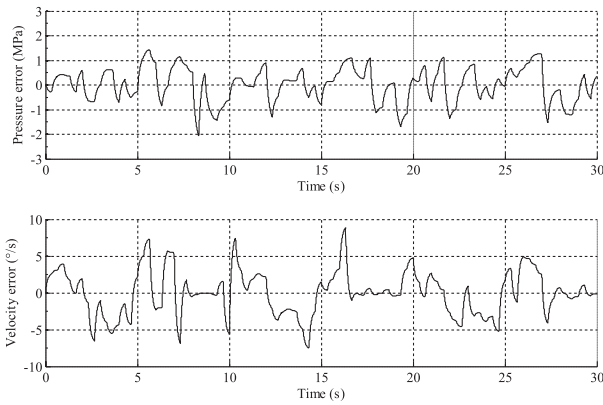


Figure 17. Tracking errors of MIMO QFT control scheme given time-variant reference inputs.

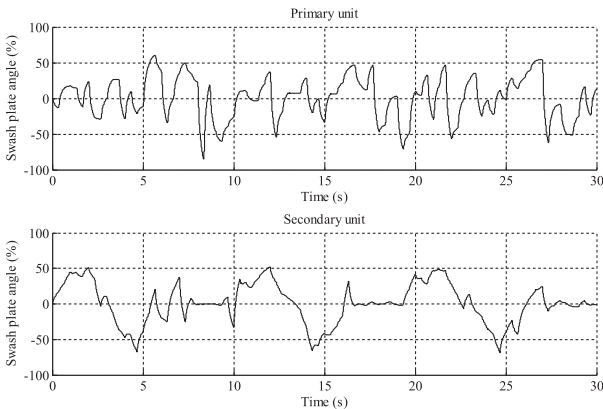


Figure 18. Swash plate angles of MIMO QFT control scheme given time-variant reference inputs.

swing system. Given that the robustness against parameter uncertainty has been verified, to show the performance level more clearly, the following evaluations are just based on the plant with nominal values.

As is seen from Figures 16 and 17, satisfactory tracking performances are obtained for both pressure and velocity responses. Due to the large inertia and fluid volume in the hydraulic hybrid swing system, there is a slight lag in pressure buildup and velocity tracking. Given that the sampling frequencies for both reference

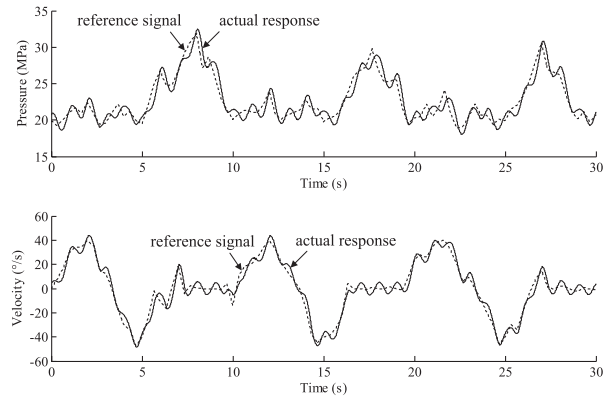


Figure 19. Tracking performances of PI control scheme with output disturbances.

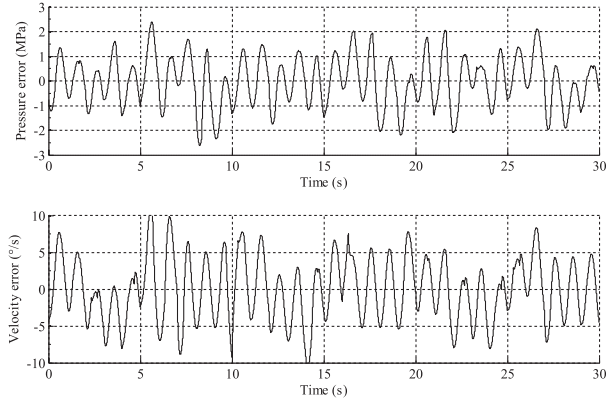


Figure 20. Tracking errors of PI control scheme with output disturbances.

signals are 3 Hz, the standard deviations between actual responses and reference signals during 30 s are 0.68 MPa and 2.98 °/s, respectively. Figure 18 shows that the swash plate angles of both primary and secondary units are also reasonable.

To further evaluate the efficacy of the proposed control laws, a PI controller is tuned to obtain similar or even slightly better tracking performances, with its standard deviations as 0.63 MPa and 2.58 °/s. The PI controller is expressed as:

$$G' = \begin{bmatrix} g'_1 \\ g'_2 \end{bmatrix} \quad (38)$$

where $g'_1 = 16.06 + \frac{1.857}{s}$, $g'_2 = 2.797 + \frac{6.993}{s}$.

With regard to sensitivity reduction, to make it as close as to the actual tough operating conditions for excavators, a set of disturbance signals are designated at the outputs of the MIMO plant. For the pressure channel, a 1 Hz sinusoidal signal with amplitude 1.5 MPa is adopted to describe the effect of environmental stiffness variations; while for the velocity channel, a 1 Hz, 10 °/s sinusoidal disturbance signal is introduced to represent the effect of gravity on tilted working surfaces.

As is seen from Figures 19–21, the tracking performances of the PI control scheme deteriorate very

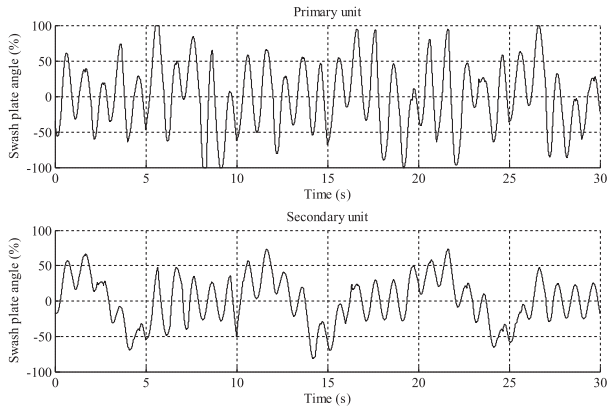


Figure 21. Swash plate angles of PI control scheme with output disturbances.

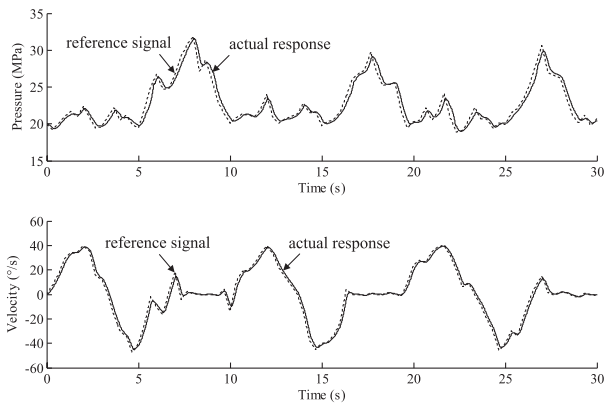


Figure 22. Tracking performances of MIMO QFT control scheme with output disturbances.

much in the presence of output disturbances. Both time responses and swash plate angles are affected greatly, with the standard deviation for pressure channel as 1.02 MPa and that for velocity as 4.34 °/s. This makes the simple PI scheme less reliable.

While employing QFT control scheme, there is not much degradation with performances. As is shown in Figures 22–24, with the pressure standard deviation as 0.71 MPa and velocity standard deviation as 2.98 °/s, it is still considered acceptable. Table 4 clearly shows that the QFT control scheme exhibits much better robustness over the PI controller.

5.3. Validity verification of the linearised model

Please note that the above-mentioned evaluation is based on the linearised state-space model derived in Section 2. To check the proposed QFT controller's constraint effect on non-linear friction and thus the validity of the linearised model, we also built up a model of the secondary controlled swing system in SimHydraulics, considering the effect of a non-linear rotational friction expressed as in Equation (3). As is seen from Figure 25, the friction level reaches a quarter of the maximum load torque, which is considered notable.

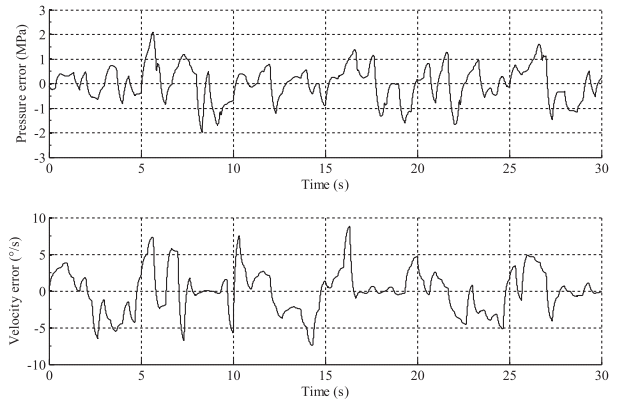


Figure 23. Tracking errors of MIMO QFT control scheme with output disturbances.

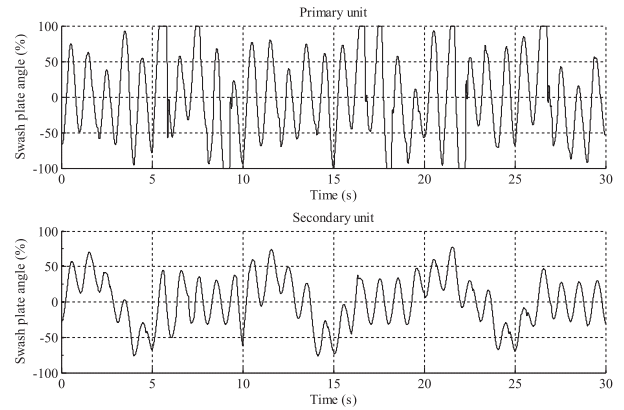


Figure 24. Swash plate angles of MIMO QFT control scheme with output disturbances.

Table 4. Standard deviations of a well-tuned PI and the proposed QFT control schemes.

Control scheme		Time-variant response	Time-variant response with disturbances	Error increase (%)
PI	Pressure (MPa)	0.63	1.02	62
	Velocity (°/s)	2.58	4.34	68
QFT	Pressure (MPa)	0.68	0.71	4
	Velocity (°/s)	2.98	2.98	0

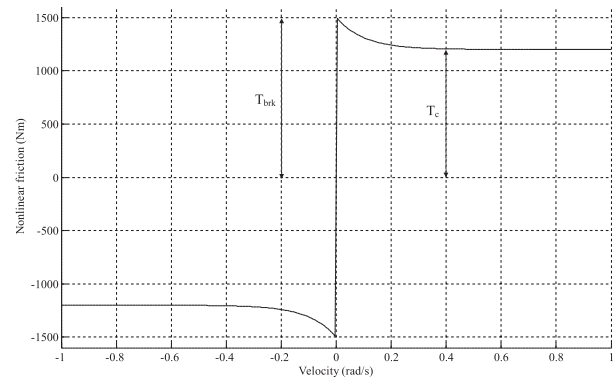


Figure 25. Non-linear friction used in SimHydraulics model.

Given the same system parameters and reference inputs, we obtain responses before and after introducing the non-linear friction in SimHydraulics. As is seen from

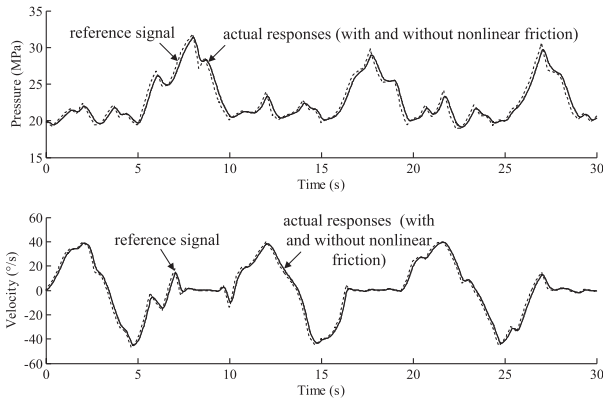


Figure 26. Tracking performances of MIMO QFT control scheme based on SimHydraulics model.

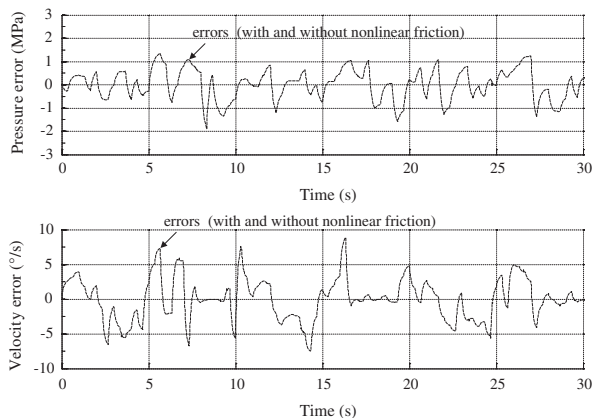


Figure 27. Tracking errors of MIMO QFT control scheme based on SimHydraulics model.

Figures 26 and 27, they show quite similar performances with that of the linearised state space model in Simulink. Without non-linear friction, the pressure standard deviation is 0.64 MPa and velocity standard deviation is 3.1 %/s. After introducing the non-linear friction, the standard deviations become 0.7 MPa and 3.2 %/s, respectively. There is very little difference that we can hardly tell the responses apart. This in turn proves the proposed QFT controller's constraint effect on non-linear friction and thus the validity of the linearised model.

6. Conclusions

Considering parametric uncertainties in load variation, viscous friction and bulk modulus, a two-input two-output QFT diagonal control scheme was synthesised for the hydraulic hybrid swing systems of excavators. Specifications of robust margin, sensitivity reduction and tracking were specified to conduct the synthesis. In simulation, with respect to step reference inputs, the prescribed robust stability and tracking specification were satisfied for the plant family. For the plant with nominal values, the settling time of pressure and velocity channels are 0.57 s and 0.43 s, respectively, and the corresponding steady-state errors are 0.004 MPa and 0.004

%/s. As to time-variant reference signals, the proposed QFT controller and a well-tuned PI controller showed similar tracking performances. In the presence of output disturbances, the pressure and velocity standard deviations of the PI controller during the duty period increased by 62 and 68%, respectively. Whereas for the MIMO QFT control scheme, the pressure standard deviation only increased by 4% and the velocity response was unaffected. This shows that the proposed QFT controller has much better robustness over the well-tuned PI controller. To conclude, the two-input two-output QFT diagonal control scheme reduced the design complexity, and exhibited excellent tracking performances and robustness in both velocity and pressure control, in the presence of parametric uncertainties and output disturbances.

Disclosure statement

No potential conflict of interest was reported by the authors.

Funding

This work was supported by Natural Sciences and Engineering Research Council of Canada [grand number RGPIN 121353-2013] and China Scholarship Council [201406080050].

Notes on contributors



Yan Cai received his BS degree in Mechanical Engineering from Northeastern University, China, in 2012. He is a direct PhD student with the School of Mechanical Engineering and Automation at Northeastern University, and is currently a PhD visiting scholar at University of Manitoba, Canada. His research interests include bilateral control, energy efficient fluid power system, robust control and automation of electro-hydraulic actuators.



Jinchun Song received his BS, MS and PhD degree in Mechanical Engineering from Northeastern University, China, in 1982, 1985 and 2004, respectively. He is a professor with the School of Mechanical Engineering and Automation at Northeastern University, China. His research interests include mechanical-electrical-hydraulic system integration, servo and proportional control of fluid power system.



Nariman Sepehri received his BS degree in Mechanical Engineering from Sharif University of Technology, Iran, in 1984, MSc and PhD degrees in Mechanical Engineering from the University of British Columbia, Canada, in 1986 and 1990, respectively. He is a professor with the Department of Mechanical and Manufacturing Engineering at University of Manitoba, Canada. He is a fellow of CAE, ASME and CSME. His research interests include fluid power systems and control, fault detection and isolation, tele-robots, modelling and simulation.

References

- Armstrong, B. and Canudas de Wit, C., 1995. *Friction modeling and compensation. The control handbook*. Boca Raton, FL: CRC Press.
- Berg, H. and Ivantysynova, M., July 1999. Design and testing of a robust linear controller for secondary controlled hydraulic drive. In: *Proceedings of the institution of mechanical engineers, part i: journal of systems and control engineering*, 213 (5), 375–386.
- Borghesani, C., Chait, Y. and Yaniv, O., 2003. *The QFT Frequency domain control design toolbox*. San Diego: Terasoft.
- Busquets, E. and Ivantysynova, M., 2014. A robust multi-input multi-output control strategy for the secondary controlled hydraulic hybrid swing of a compact excavator with variable accumulator pressure. In: *The ASME/BATH 2014 symposium on fluid power and motion control*, 10–12 September, Bath, 1–9.
- Busquets, E. and Ivantysynova, M., 2015. Adaptive robust motion control of an excavator hydraulic hybrid swing drive. *SAE international journal of commercial vehicles*, 8 (2), 568–582.
- Caterpillar, 2012. *Caterpillar unveils first hybrid excavator* [online]. Available from: http://www.cat.com/en_US/news/machine-press-releases/caterpillar-unveilsfirsthybridexcavator.html [Accessed 18 July 2016].
- Chait, Y. and Hollot, C.V., 1990. A comparison between H-infinity methods and QFT for a SISO plant with both parametric uncertainty and performance specifications. In: O.D.I. Nwokah, ed. *Recent development in quantitative feedback theory*. 33–40.
- Hippalgaonkar, R. and Ivantysynova, M., 2013. A series-parallel hydraulic hybrid mini-excavator with displacement controlled actuators. In: *The 13th Scandinavian international conference on fluid power (SICFP2013)*, 3–5 June, Linköping, 31–42.
- Ho, T.H. and Ahn, K.K., 2012. Design and control of a closed-loop hydraulic energy-regenerative system. *Automation in Construction*, 22, 444–458.
- Inoue, H., 2008. Introduction of PC200-8 hybrid hydraulic excavators. *Komatsu technical report*, 54 (161), 1–6.
- Jin, K., Park, T. and Lee, H., 2012. A control method to suppress the swing vibration of a hybrid excavator using sliding mode approach. *Proceedings of the institution of mechanical engineers, Part C: Journal of mechanical engineering science*, 226 (5), 1237–1253.
- Kagoshima, M., et al., 2007. Development of new hybrid excavator. *Kobelco technology review*, 27, 39–42.
- Tae-Suk Kwon, T.-S., et al., 2010. Power Control Algorithm for Hybrid Excavator With Supercapacitor. *IEEE Transactions on Industry Applications*, 46 (4), 1447–1455.
- Lee, J.W., Chait, Y. and Steinbuch, M., 2000. On QFT tuning of multivariable μ controllers. *Automatica*, 36 (11), 1701–1708.
- Lin, T.L., et al., 2010a. Research on the energy regeneration systems for hybrid hydraulic excavators. *Automation in construction*, 19 (8), 1016–1026.
- Lin, T.L., et al., 2010b. Development of hybrid powered hydraulic construction machinery. *Automation in construction*, 19 (1), 11–19.
- Ochiai, M. and Ryu, S., 2008. Hybrid in construction machinery. In: *The 7th JFPS international symposium on fluid power*, 15–18 September, Toyama, 41–44.
- Pettersson, K., 2009. *Secondary controlled swing drive*. Thesis (MS). Linköping University.
- Pettersson, K. and Tikkanen, S., 2009. Secondary control in construction machinery - design and evaluation of an excavator swing drive. In: *The 11th Scandinavian international conference on fluid power (SICFP'09)*, 2–4 June, Linköping.
- Vukovic, M. and Murrenhoff, H., 2015. The next generation of fluid power systems. *Procedia engineering*, 106, 2–7.
- Wang, Q.F., Zhang, Y.T. and Xiao, Q., 2005. Evaluation for energy saving effect and simulation research on energy saving of hydraulic system in hybrid construction machinery. *Chinese journal of mechanical engineering*, 41 (12), 135–140.
- Williamson, C., Zimmerman, J., and Ivantysynova, M., 2008. Efficiency study of an excavator hydraulic system based on displacement-controlled actuators. In: *Bath/ASME symposium on fluid power and motion control (FPMC2008)*, Bath, 291–307.
- Xiao, Q., Wang, Q.F. and Zhang, Y.T., 2008. Control strategies of power system in hybrid hydraulic excavator. *Automation in construction*, 17 (4), 361–367.
- Yaniv, O., 1999. *Quantitative feedback design of linear and nonlinear control systems*. Norwell, MA: Kluwer Academic.
- Yao, B., et al., 1998. High performance swing velocity tracking control of hydraulic excavators. In: *The 1998 American control conference*, June, Philadelphia, 2, 818–822.
- Yoon, J., Truong, D.Q. and Ahn, K.K., 2013. A generation step for an electric excavator with a control strategy and verifications of energy consumption. *International journal of precision engineering and manufacturing*, 14 (5), 755–766.
- Zimmerman, J., Hippalgaonkar, R. and Ivantysynova, M., 2011. Optimal control for the series-parallel displacement controlled hybrid excavator. In: *The ASME 2011 dynamics systems and control conference and Bath/ASME symposium on fluid power and motion control*, 31 October–2 November, Arlington, 1, 129–136.